Supplemental Information

Atomically Visualizing Elemental Segregation Induced Surface Alloying and Restructuring

Lianfeng Zou[1], Jonathan Li[2], Dmitri Zakharov[3], Wissam A. Saidi[4], Eric A. Stach[3], Guangwen Zhou[1*]

[1]Department of Mechanical Engineering & Materials Science and Engineering Program, State University of New York at Binghamton, NY 13902

[2]Department of Physics, Applied Physics and Astronomy & Materials Science and Engineering Program, State University of New York, Binghamton, NY 13902

[3]Center for Functional Nanomaterials, Brookhaven National Laboratory, Upton, NY 11973

[4]Department of Mechanical Engineering and Materials Science, University of Pittsburgh, Pittsburgh, PA 15261

This file includes:

Other Supplementary Materials for this manuscript includes the following:

Supplemental Videos 1 to 3

1. TEM experiments and sample preparation

The surface segregation experiments were performed in a dedicated environmental TEM (FEI Titan 80-300) equipped with an objective-lens aberration corrector. Single-crystal Cu-10at.%Au(100) thin films with a nominal thickness of ~50 nm were grown on NaCl using e-beam co-evaporation of Cu and Au. The alloy films were transferred from the NaCl substrate by flotation in deionized water, washed, and mounted onto a TEM specimen holder. As TEM imaging is a two-dimensional (2D) projection view of a 3D object along the direction of the transmitted electron beam, the surface information overlaps with the bulk and cannot be resolved along the planar view direction. We overcome this issue by annealing the Cu-Au films at 600 °C and in a $pH_2 = 1\times10^{-3}$ Torr of H_2 gas flow, which resulted in the removal of native oxide and the formation of faceted holes in the thin film [1-4]. These freshly created facets are atomically clean and ideal for cross-sectional TEM observations of structural changes in the surface and subsurface regions. The TEM observations of dynamics of surface-segregation induced structural changes were performed at 350 ^{o}C, which is below the bulk Cu_3Au and CuAu order-disorder transition temperatures, which are 390 ^{o}C and 412 ^{o}C, respectively.

2. Identification of Cu and Au arrangement at the (420) surface

We performed HRTEM image simulation to ascertain the origin of the atomic column contrast difference between each atomic column at the surface and subsurface region, by assigning the Cu and Au atoms at each column of the (420) facet. The simulated HRTEM images (Fig. S1(b)) obtained using the Cu and Au arrangement as shown in Fig. 4(a) consistently reproduced the characteristically darker Au atom contrast for the alternative columns of the (100) terrace of the (420) facet relative to the neighboring column (Fig. S1(a)). Experimental parameters used in the HRTEM image simulation: accelerating voltage: 300 kV, spherical aberration coefficient: 1 um, defocus spread: 45 Å, beam convergence: 0.001 $Å^{-1}$, defocus value: 85 nm. Effects of thermally induced atomic motion are included in our HRTEM simulation by the Debye-Waller factors, which are calculated to be 1.2 and 1, respectively, for Cu and Au at 350 °C.

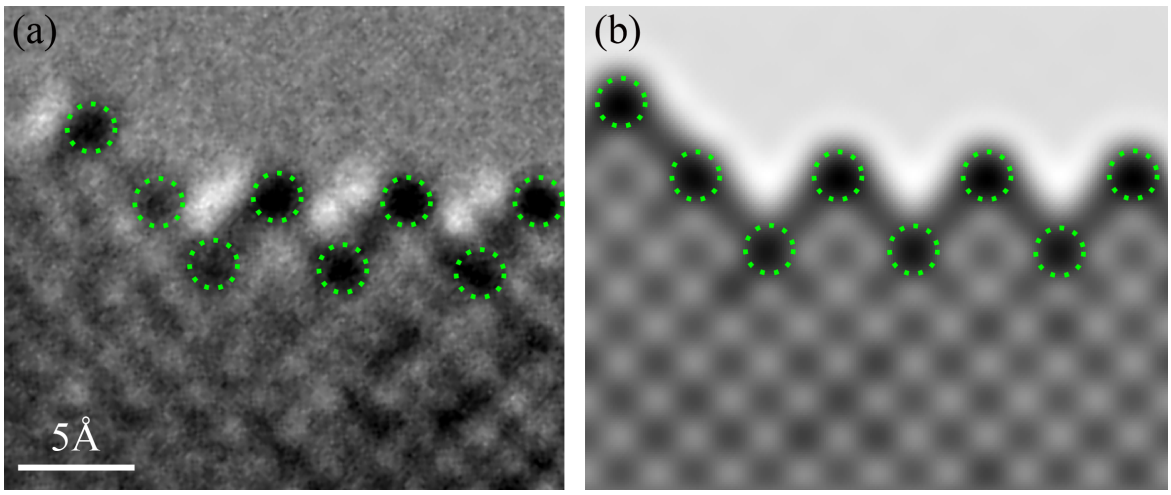

Fig. S1: Identification of the Cu and Au columns of (420) surface. (a) HRTEM image showing the alternative dark columns at the (100) terrace of (420) facet. (b) Simulated HRTEM image based on the atomic model in Fig. 4(a). The simulations reproduce the dark contrast of Au columns at the every other column of the (100) terrace. Green dotted circles outline Au atom columns.

3. DFT calculations

The DFT calculations were performed using the Vienna ab initio simulation package [5, 6] with the PW91 generalized gradient approximation [7] and projector-augmented wave potentials [8] using a cutoff energy of 400 eV. The calculations were carried out with broadening of the Fermi surface according to Methfessel–Paxton smearing technique [9] with a smearing parameter of 0.2 eV. The structural optimization is terminated when all force components acting on the unconstrained atoms are less than 0.01 eV/Å, while the bottom 4 layers are fixed and the rest of the atoms are free to relax. The Brillouin zone is sampled using a 2 × 12 × 1 Monkhorst–Pack mesh [10]. We calculated the lattice constant of Cu to be 3.64 Å.

The models shown in Fig. S2 represent the slab models based on the (420) surface with the (110)-(2×1) reconstructed surface, where Fig. S1(a) contains both Au and Cu at the surface and Fig. S2(b) contains pure Cu. The vacancy formation energy E_{vac} is calculated using the equation

$$E_{vac} = E_{ref} - E_{tot} + E_{atom}$$

where E_{tot} is the total energy of the system(with removed atom), E_{ref} is the energy of the structure before removal of the atom, and E_{atom} is the is the energy of either a single Cu or Au atom in the bulk.

To assess the surface stability, we sequentially remove step-by-step atoms labeled in Fig. S2. Each labeled site that is removed in Table S1 includes the removal of the atoms that proceed the specified atom. For example, the vacancy formation energy calculated for Site 2 is the removal of atom 2, where the reference structure has atom 1 already removed.

Table S1. The vacancy formation energies of atoms corresponding to labeled atoms in Fig. S2. Model 1 represents Fig. S2(a) and Model 2 represents Fig. S2(b).

Site	Vacancy Formation Energy (eV)	
	Model 1	Model 2
1	0.29	
2	0.02	
3	-0.30	
4	0.15	
5	0.28	-0.33
6	0.07	0.29

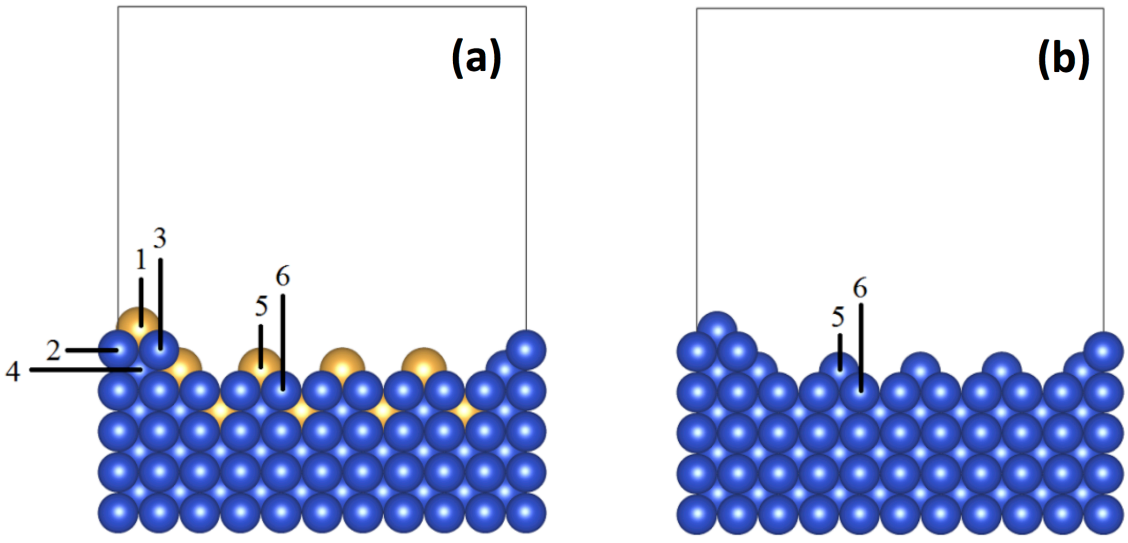

Fig. S2: Models of the (420) and (110)-(2×1) surfaces consisting of (a) Cu and Au on the surface, and (b) pure Cu. The blue balls represent Cu atoms and the yellow balls represent Au atoms.

References:

1. Zhou, G.; Luo, L.; Li, L.; Ciston, J.; Stach, E. A.; Saidi, W. A.; Yang, J. C. In-Situ Atomic-Scale Visualization of Oxide Islanding during Oxidation of Cu Surfaces. *Chem. Commun.* **2013,** *49* (92), 10862-10864.

2. Zhou, G.; Luo, L.; Li, L.; Ciston, J.; Stach, E. A.; Yang, J. C. Step-Edge-Induced Oxide Growth during the Oxidation of Cu Surfaces. *Phys. Rev. Lett.* **2012,** *109* (23), 235502.

3. Zou, L.; Li, J.; Zakharov, D.; Stach, E. A.; Zhou, G. In Situ Atomic-Scale Imaging of the Metal/Oxide Interfacial Transformation. *Nat. Commun.* **2017,** *8* (1), 307.

4. Li, L.; Luo, L.L.; Ciston, J.; Saidi, W.A.; Stach, E.A.; Yang, J.C.; Zhou, G.W. Surface-Step-Induced Oscillatory Oxide Growth. *Phys. Rev. Lett.* **2014**, 113 (13), 136104.

5. Kresse, G.; Hafner, J. Ab initio molecular-dynamics simulation of the liquid-metal–amorphous-semiconductor transition in germanium. *Phys. Rev. B* **1994,** *49* (20), 14251.

6. Kresse, G.; Furthmüller, J. Efficiency of Ab-Initio Total Energy Calculations for Metals and Semiconductors using a Plane-Wave Basis Set. *Comput. Mater. Sci.* **1996,** *6* (1), 15-50.

7. Perdew, J. P.; Chevary, J. A.; Vosko, S. H.; Jackson, K. A.; Pederson, M. R.; Singh, D. J.; Fiolhais, C. Atoms, Molecules, Solids, and Surfaces: Applications of the Generalized Gradient Approximation for Exchange and Correlation. *Phys. Rev. B* **1992,** *46* (11), 6671.

8. Kresse, G.; Joubert, D. From Ultrasoft Pseudopotentials to the Projector Augmented-Wave Method. *Phys. Rev. B* **1999,** *59* (3), 1758.

9. Methfessel, M.; Paxton, A. High-Precision Sampling for Brillouin-Zone Integration in Metals. *Phys. Rev. B* **1989,** *40* (6), 3616.

10. Monkhorst, H. J.; Pack, J. D. Special Points for Brillouin-Zone Integrations. *Phys. Rev. B* **1976,** *13* (12), 5188.

Captions for Supplementary in-situ TEM videos

Supplemental in-situ TEM video 1: In-situ TEM video showing the Au-segregation induced nucleation and growth of the half-unit-cell-thick $Cu_3Au(110)$-(2×1) surface alloy out of the Cu-10at.%Au solid solution

Supplemental in-situ TEM video 2: In-situ TEM video showing the (410)→(420) →(2×1) structural transition pathway leading to the growth of the (2×1) reconstructed Cu_3Au surface alloy

Supplemental in-situ TEM video 3: In-situ TEM video showing the sequential detachment of Cu and Au atoms in pairs from the half-unit-cell-thick $Cu_3Au(110)$-(2×1) surface alloy